



**HAL**  
open science

# Thermal Tides in the Martian Atmosphere Near Northern Summer Solstice Observed by ACS/TIRVIM Onboard TGO

Siteng Fan, Sandrine Guerlet, Francois, Forget, Antoine Bierjon, Ehouarn Millour, Nikolay Ignatiev, Alexey Shakun, Alexey Grigoriev, Alexander Trokhimovskiy, Franck Montmessin, et al.

## ► To cite this version:

Siteng Fan, Sandrine Guerlet, Francois, Forget, Antoine Bierjon, Ehouarn Millour, et al.. Thermal Tides in the Martian Atmosphere Near Northern Summer Solstice Observed by ACS/TIRVIM Onboard TGO. *Geophysical Research Letters*, 2022, 49 (7), pp.e2021GL097130. 10.1029/2021GL097130 . insu-03619922v2

**HAL Id: insu-03619922**

**<https://insu.hal.science/insu-03619922v2>**

Submitted on 24 Apr 2022

**HAL** is a multi-disciplinary open access archive for the deposit and dissemination of scientific research documents, whether they are published or not. The documents may come from teaching and research institutions in France or abroad, or from public or private research centers.

L'archive ouverte pluridisciplinaire **HAL**, est destinée au dépôt et à la diffusion de documents scientifiques de niveau recherche, publiés ou non, émanant des établissements d'enseignement et de recherche français ou étrangers, des laboratoires publics ou privés.

# Geophysical Research Letters<sup>®</sup>



## RESEARCH LETTER

10.1029/2021GL097130

### Special Section:

ExoMars Trace Gas Orbiter -  
One Martian Year of Science

## Thermal Tides in the Martian Atmosphere Near Northern Summer Solstice Observed by ACS/TIRVIM Onboard TGO

Siteng Fan<sup>1</sup> , Sandrine Guerlet<sup>1,2</sup> , François Forget<sup>1</sup>, Antoine Bierjon<sup>1</sup>, Ehouarn Millour<sup>1</sup>, Nikolay Ignatiev<sup>3</sup>, Alexey Shakun<sup>3</sup> , Alexey Grigoriev<sup>4</sup>, Alexander Trokhimovskiy<sup>3</sup> , Franck Montmessin<sup>5</sup> , and Oleg Korabiev<sup>3</sup> 

### Key Points:

- Thermal tides in the Martian atmosphere are investigated using temperature profiles retrieved from TIRVIM nadir observations
- Diurnal tide dominates daily temperature variations; semi-diurnal tide and diurnal Kelvin wave are also important
- Observations agree well with numerical simulations, but suggest phases of diurnal and semi-diurnal tides earlier than predicted

### Supporting Information:

Supporting Information may be found in the online version of this article.

### Correspondence to:

S. Fan,  
[sfan@lmd.ipsl.fr](mailto:sfan@lmd.ipsl.fr)

### Citation:

Fan, S., Guerlet, S., Forget, F., Bierjon, A., Millour, E., Ignatiev, N., et al. (2022). Thermal tides in the Martian atmosphere near northern summer solstice observed by ACS/TIRVIM onboard TGO. *Geophysical Research Letters*, 49, e2021GL097130. <https://doi.org/10.1029/2021GL097130>

Received 19 NOV 2021  
Accepted 19 MAR 2022

<sup>1</sup>LMD/IPSL, Sorbonne Université, PSL Research Université, École Normale Supérieure, École Polytechnique, CNRS, Paris, France, <sup>2</sup>LESIA, Observatoire de Paris, CNRS, Sorbonne Université, Université Paris-Diderot, Meudon, France, <sup>3</sup>Space Research Institute (IKI), Moscow, Russia, <sup>4</sup>Research School of Astronomy and Astrophysics, Australian National University, Canberra, ACT, Australia, <sup>5</sup>LATMOS/IPSL, Guyancourt, France

**Abstract** Thermal tides in the Martian atmosphere are analyzed using temperature profiles retrieved from nadir observations obtained by the TIRVIM Fourier-spectrometer, part of the Atmospheric Chemistry Suite onboard the ExoMars Trace Gas Orbiter. The data is selected near the northern summer solstice at solar longitude ( $L_s$ ) 75°–105° of Martian Year 35. The observations have a full local time coverage, which enables analyses of daily temperature anomalies. The observed zonal mean temperature is lower by 4–6 K at ~100 Pa, but higher toward the summer pole, compared to the Laboratoire de Météorologie Dynamique (LMD) Mars General Circulation Model (GCM). Wave mode decomposition shows dominant diurnal tide and important semi-diurnal tide and diurnal Kelvin wave, with maximal amplitudes of 5, 3, and 2.5 K, respectively, from tens to hundreds of Pa. The results generally agree well with the LMD Mars GCM, but with noticeable earlier phases of diurnal (~1 hr) and semi-diurnal (~3 hr) tides.

**Plain Language Summary** Unlike the Earth, daily temperature variation on Mars is as large as tens of degrees because of its thin atmosphere. The sunlight absorbed by the Martian surface and dust in the atmosphere leads to dramatic temperature increase in the lower atmosphere during daytime. Such large and regular changes can trigger temperature waves, and some modes of them can propagate into higher altitudes, where they become the major factor controlling the daily temperature variation. In this work, temperature profiles obtained using thermal-infrared spectra are analyzed. Zonal mean temperature is compared with numerical simulations of the Martian atmosphere. Different types of the wave modes are computed through decomposition. Results from the observation agree well with model prediction when the observation mechanisms are taken into consideration. Estimation of the strength of these waves can be improved in the future with improved design of observation strategies.

## 1. Introduction

Atmospheric thermal tides are planetary-scale harmonic responses driven by diurnal solar forcing and influenced by planetary topography (Gierasch & Goody, 1968; Zurek, 1976). As results of solar heating absorbed directly by the atmosphere and exchanged with the surface, thermal tides in the Martian atmosphere usually have large amplitudes due to its low heat capacity, and dominate the diurnal temperature variations throughout the thin atmosphere. Among the excited tides, some modes can vertically propagate into the middle and upper atmospheres with amplitudes growing exponentially with decreasing air density, which therefore influences the mean atmospheric circulation.

Diurnal temperature variations and related pressure changes have been observed by many Mars landers and orbiters (e.g., Banfield et al., 2000; Forbes et al., 2020; Hess et al., 1977; Kleinböhl et al., 2013; Lee et al., 2009), which have significantly enriched our knowledge of the Martian thermal tides in the past two decades. However, many recent Mars missions have had sun-synchronous orbits, where temperature observations are mostly limited to two local times which differ by half of a Martian solar day (sol), for example, 2 and 14 hr for the Thermal Emission Spectrometer (TES) onboard the Mars Global Surveyor (MGS, Banfield et al., 2000), and 3 and 15 hr for the Mars Climate Sounder (MCS) onboard the Mars Reconnaissance Orbiter (MRO), despite some offsets of ±1.5–3.0 hr of cross-track observations (Forbes et al., 2020; Kleinböhl et al., 2013). Mars Express has been in

© 2022 The Authors.

This is an open access article under the terms of the [Creative Commons Attribution-NonCommercial License](https://creativecommons.org/licenses/by-nc/4.0/), which permits use, distribution and reproduction in any medium, provided the original work is properly cited and is not used for commercial purposes.

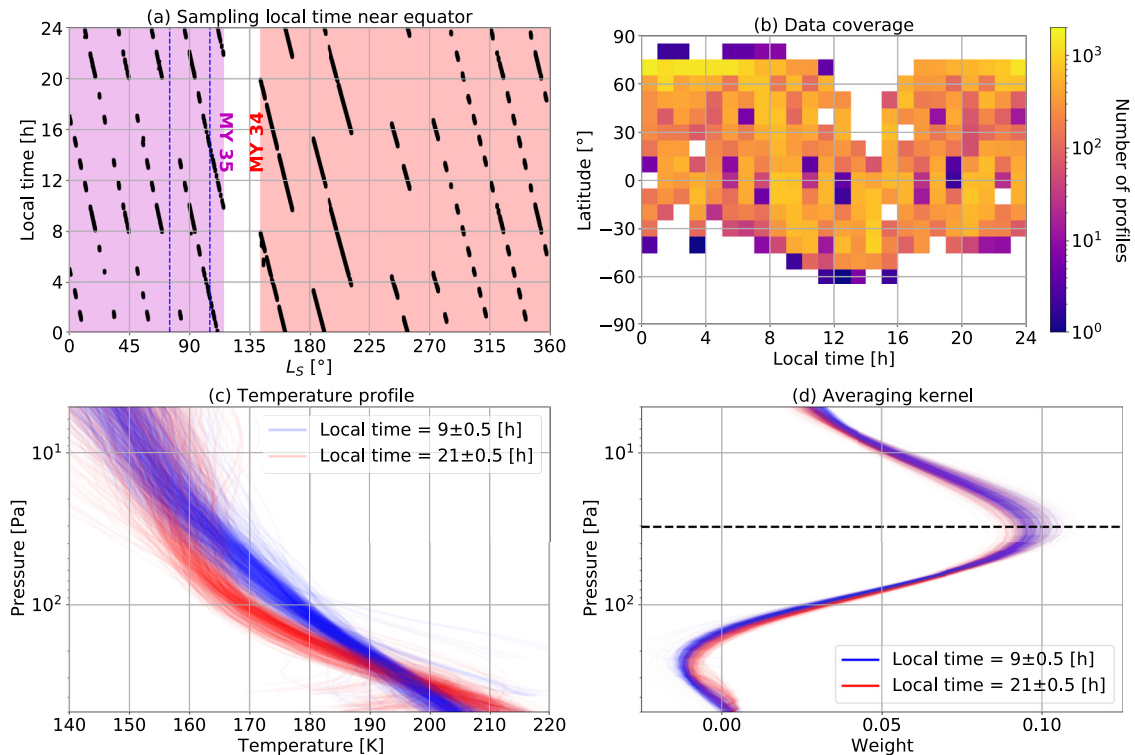


**Figure 1.** (a) Season and local time of TIRVIM temperature profile observations between  $\pm 5^\circ$  in latitude (back dots). The two shaded areas denote MY 34 (red) and MY 35 (magenta). The two blue vertical dashed lines denote the season ( $L_S = 75^\circ\text{--}105^\circ$ ) selected in this work. (b) Numbers of TIRVIM temperature profiles in the (latitude, local time) bins. (c) Temperature profiles between  $\pm 5^\circ$  in latitude and within half an hour of 9 (blue) and 21 hr (red) in local time. (d) Averaging kernels of retrieving the temperatures at 30 Pa (black dashed line) using observations between  $\pm 5^\circ$  in latitude and within half an hour of 9 (blue) and 21 hr (red) in local time.

a non-solar-synchronous polar orbit, but its large orbital inclination only allowed it to monitor the diurnal cycle using the Planetary Fourier Spectrometer (PFS) within a long period comparable to a Martian year (MY) to cover all local times (Giuranna et al., 2021). Analyses using sun-synchronous observations can reasonably investigate the diurnal tide, while constraints on aliasing waves, especially those with even number in temporal frequency, require plenty of a priori knowledge about the latitude-pressure structure of each wave mode predicted by the tidal theory (e.g., Guzewich et al., 2012). Therefore, data with large local time and spatial coverage are required for analysis of such planetary-scale diurnal/sub-diurnal variations. Observations by TIRVIM can meet these requirements, which is the subject of this work.

## 2. Observations and Data Processing

### 2.1. Instrument and Observations

TIRVIM is a double-pendulum Fourier-spectrometer, one of the three instruments of the Atmospheric Chemistry Suite (ACS) onboard the ESA-Roscosmos mission ExoMars Trace Gas Orbiter (TGO, Korabev et al., 2018; Svedhem et al., 2020). The spacecraft is in a near-circular orbit with a radius of  $\sim 400$  km and a period of  $\sim 2$  hr (Capderou & Forget, 2004). The orbit is not sun-synchronous, and the sub-spacecraft point slowly drifts in local time (Figure 1a). A full diurnal cycle can be sampled in nadir viewing geometry between  $74^\circ\text{N}$  and  $74^\circ\text{S}$  within  $\sim 55$  sols, which is equivalent to  $\sim 30^\circ$  in solar longitude ( $L_S$ ). Details of the TIRVIM instrument are presented in Korabev et al. (2018). Through nadir sounding, TIRVIM is designed to monitor the temperature in the Martian atmosphere and of the surface, as well as column integrated aerosols (dust and clouds). Under this observation scheme, the instrument is sensitive to thermal infrared from  $620$  to  $1300\text{ cm}^{-1}$  with a spectral resolution of  $1.2\text{ cm}^{-1}$ . TIRVIM operated from April 2018 to December 2019, nearly one MY from MY34  $L_S = 134^\circ$  to MY35  $L_S = 115^\circ$ . It provided  $\sim 1.7$  million thermal infrared spectra with decent data quality. Guerlet et al. (2022) presented a retrieval process based on optimal estimation theory that simultaneously retrieves atmospheric temperature profile, surface temperature, and the optical depths of dust and water ice clouds from these spectra.

It builds initial guess of the temperatures using different parts of TIRVIM spectra (660–740  $\text{cm}^{-1}$  for atmospheric and 1240–1290  $\text{cm}^{-1}$  for surface temperature), and then it iterates with a radiative transfer model until the synthetic spectrum converges to the observed one or the maximal number (10) of iterations is reached. The derived temperature profiles typically cover a vertical range from  $\sim 2$  to 3 km above Mars' surface to  $\sim 50$ –55 km ( $\sim 1$ –2 Pa) with a vertical resolution of  $\sim 1$  scale height (10 km) and a typical retrieval error of  $\sim 2$  K at pressure  $> 30$  Pa. These temperature profiles cover most local time within sub-seasonal scales (Figure 1b), which enables the investigation of thermal tides on a sub-daily basis and resolves the harmonic aliasing.

## 2.2. Data Processing

Temperature profiles used for analysis in this work are selected near the northern summer solstice during  $L_s = 75^\circ$ – $105^\circ$  of MY35, which totals  $\sim 9.5 \times 10^4$  in number (Guerlet, 2021). This is a clear season with no dust storms identified, so the temperature structure of the atmosphere is not expected to undergo drastic changes. As the observations are not evenly distributed at different local times and locations (Figure 1b), individual profiles are first binned with grid sizes of 5, 10, and 1 hr in longitude, latitude, and local time, respectively, to derive zonal-mean daily temperatures, and corresponding daily anomalies which are shown in Section 3.2. Each bin is assumed to have the same weight so that the sampling bias in local time and location can be decreased. In the wave mode decomposition (Section 2.3 and 3.3), however, only the latitude bin is included as the local time and the longitude are considered directly.

## 2.3. Wave Mode Decomposition

To investigate the contributions of each wave mode, temperature at a given latitude and pressure level is assumed to be a linear combination of waves as shown in Equation 1, and then different modes of waves could be decomposed accordingly using least-square fit, in line with previous works (e.g., Banfield et al., 2000, Lee et al., 2009, Wu et al., 2015, 2017).

$$T(\lambda, \varphi, p, t) = \sum_{\sigma, s} (C_{\sigma, s}(\varphi, p) \cos(s\lambda + \sigma t) + S_{\sigma, s}(\varphi, p) \sin(s\lambda + \sigma t)) \quad (1)$$

where  $\lambda$ ,  $\varphi$ , and  $p$  are longitude, latitude, and pressure level, respectively;  $t$  is the universal time;  $s$  and  $\sigma$  are the frequencies in longitude and time;  $C$  and  $S$  are the coefficients of the cosine and sine functions at a certain latitude and pressure level, which are the unknowns in the decomposition. Positive values of  $s/\sigma$  denote westwards propagating waves; for example,  $(s, \sigma) = (1, 1)$  indicates the mode with wavenumber one in longitude and period of one Martian day in time, which is the diurnal tide. Temperature profiles are binned in latitude, and within each latitude bin individual temperature profiles are considered with the same weight in the decomposition to compute the corresponding coefficients ( $C$  and  $S$ ) of this latitude bin. Applying the decomposition to the three-dimensionally binned data has similar results if each bin is weighted by corresponding observation numbers, but using individual profiles leads to more precise values of time and location. The truncation of the expansion is selected as  $s = \{0, 1, 2, 3\}$  and  $\sigma = \{-2, -1, 0, 1, 2\}$ , which is the same as Wu et al. (2015, 2017). This results in 35 linearly independent unknowns of  $C$  and  $S$  at each pressure level in a given latitude bin, which typically consists of thousands of temperature observations. Higher order waves are ignored as their contributions are thought to be negligible. Amplitude ( $A$ ) and phase ( $\theta$ ) of each mode can finally be obtained by combining the coefficients.

$$A_{\sigma, s}(\varphi, p) = \sqrt{C_{\sigma, s}(\varphi, p)^2 + S_{\sigma, s}(\varphi, p)^2} \quad (2)$$

$$\theta_{\sigma, s}(\varphi, p) = \tan^{-1} \left( \frac{C_{\sigma, s}(\varphi, p)}{S_{\sigma, s}(\varphi, p)} \right) \quad (3)$$

## 3. Results

### 3.1. Temperature Profiles

Example temperature profiles obtained near 9 and 21 hr between  $\pm 5^\circ$  in latitude are shown in Figure 1c. Profiles at these two local times show consistent differences. The atmosphere is warmer at 21 hr near the surface, while

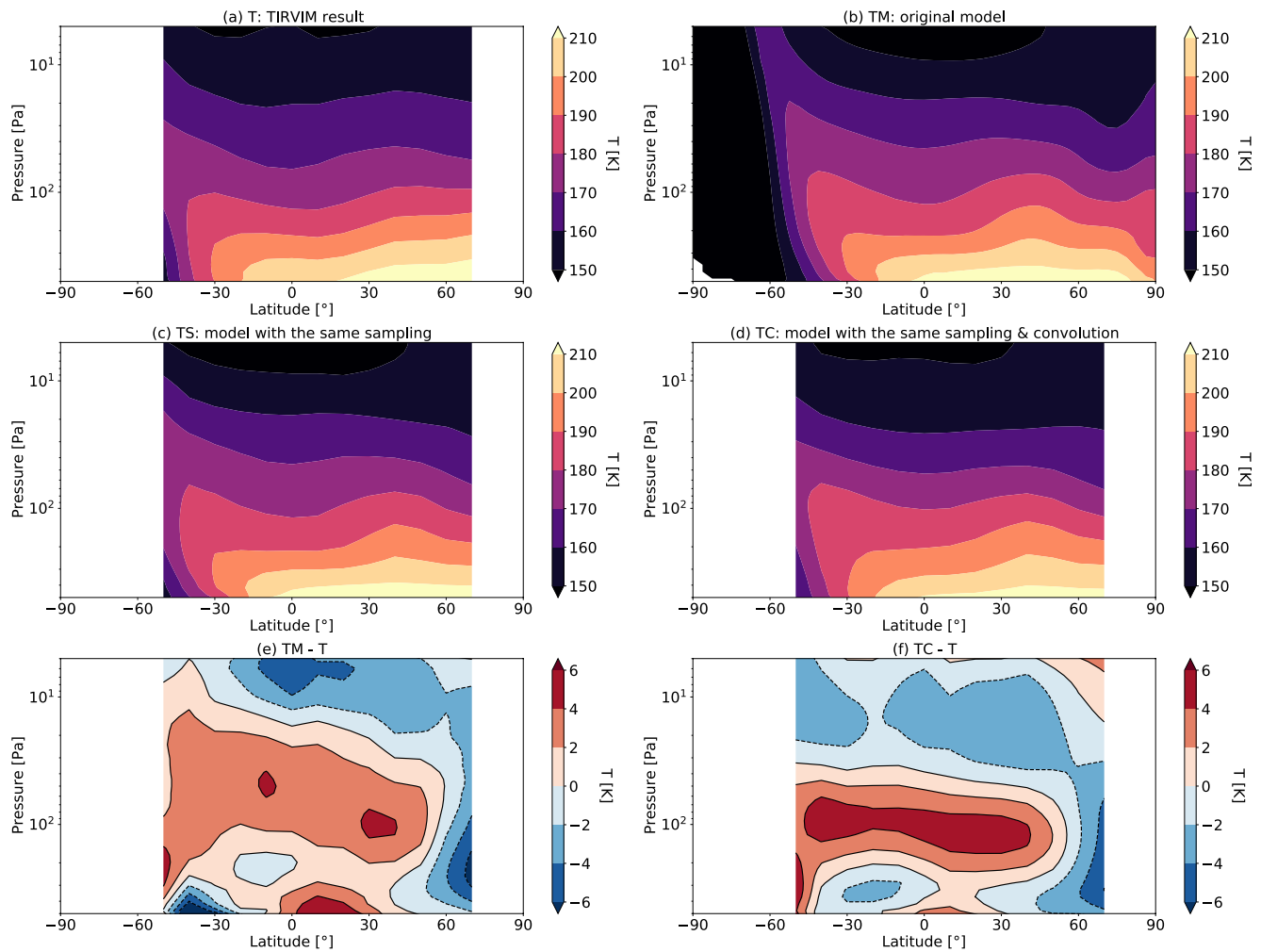


**Figure 2.** (a) Zonal and diurnal mean temperature computed using TIRVIM observations during MY 35  $L_S = 75^\circ\text{--}105^\circ$ . (b) Same as (a), but for the LMD Mars General Circulation Model (GCM) outputs. (c) Same as (b), but the outputs are sampled at the same locations and times as TIRVIM observations. (d) Same as (c), but it includes the vertical convolution. (e) Difference of the zonal and diurnal mean temperature between observations and the original GCM outputs, which is the difference between (a) and (b). (f) Same as (e), but for the difference between (a) and (d), where the GCM outputs are sampled and convolved the same way as observations.

colder at  $\sim 100$  Pa. As a result of nadir sounding, temperature retrieved at a specific pressure level is a weighted average of a large vertical region, for example,  $\sim 10\text{--}80$  Pa for temperature retrieved at 30 Pa (Figure 1d), so the temperature profiles are smoother than those retrieved using limb sounding, for example, MCS (Lee et al., 2009). However, differences among the temperature profiles obtained at these two local times are consistently monitored, as the vertical convolution does not vary much with local time (Figure 1d). More details and examples are discussed in Guerlet et al. (2022).

### 3.2. Zonal Mean Daily Temperature

To investigate the zonal mean daily temperature, the binned data are averaged along the longitude dimension, then diurnal mean and anomaly are derived. Results of the observed diurnal mean temperature show a typical solstice distribution (Figure 2a), including an indication of warming at tens of Pa toward the winter pole due to the downwelling branch of the Hadley circulation. Prediction of such observation using the Laboratoire de Météorologie Dynamique (LMD) Mars Global Circulation Model (GCM, Forget et al., 1999; Fan, 2022) is given in Figure 2b, which is computed by binning the outputs over  $L_S = 75^\circ\text{--}105^\circ$ . Description of the GCM is given in Text S1 in the Supporting Information S1. The diurnal mean temperature distribution does not change much when the model outputs are sampled at the same locations and times as observations (Figure 2c), and with vertical convolution

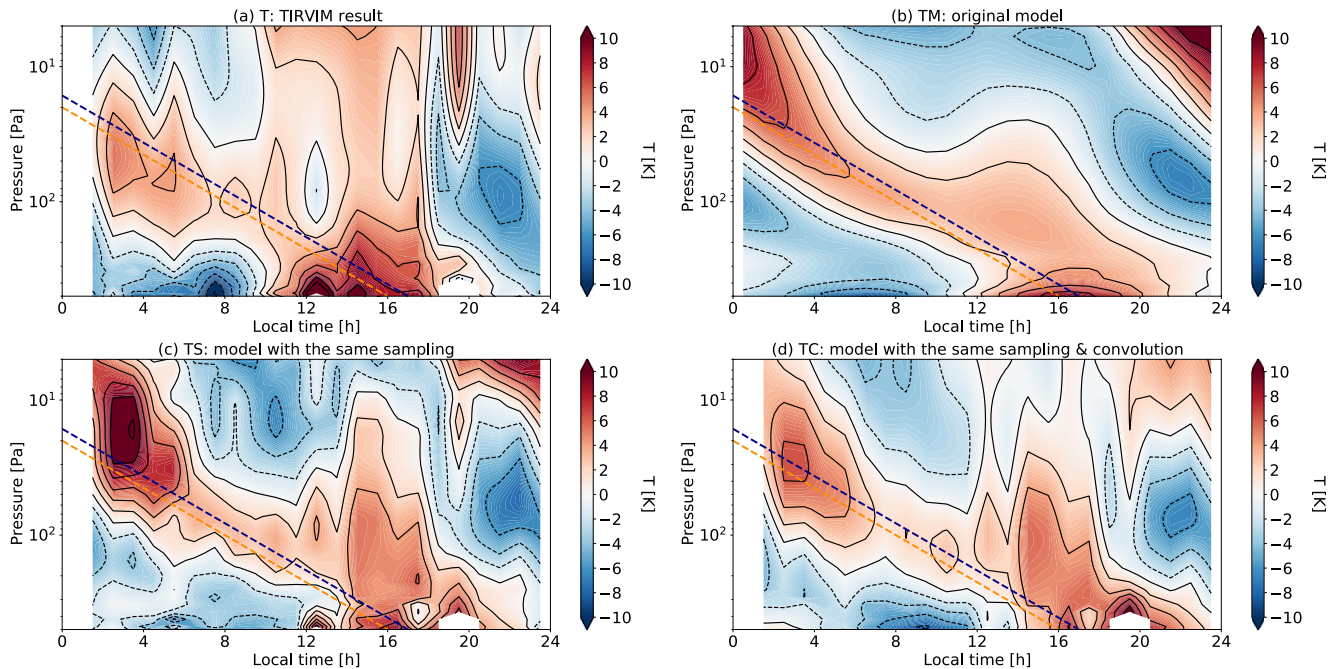


**Figure 3.** Same as Figures 2a–2d, but for zonal mean daily temperature anomaly between  $\pm 5^\circ$  in latitude. The orange and blue dashed lines denote the approximate slope of the downward phase progression of temperature maximum for observations and model outputs, respectively, which differ by 1 hr in local time. Model–observation comparison should be done by comparing (a) and (d).

considered (Figure 2d). These two factors are important in the investigation of diurnal anomalies (see below). The GCM prediction shows a good agreement with observations, but with noticeable differences (Figure 2e), and these differences are more consistent when the observation scheme is considered (Figure 2f). Compared to the TIRVIM results, the model is warmer by 4–6 K near 100 Pa, and slightly colder above, while the temperature toward the summer pole is consistently underestimated with a difference of 4–6 K from the surface to tens of Pa. These differences are likely due to the challenges of simulating physical processes in the GCM, for example, dust and/or water clouds (Navarro et al., 2017), and are indications and constraints for further model improvement.

Daily temperature anomalies are obtained by subtracting the diurnal mean from temperature profiles. An example in the equatorial region between  $\pm 5^\circ$  latitude is given in Figure 3a. It is the first time that such diurnal variations in the Martian atmosphere are observed at almost all local times within a Martian season. It shows a signature of diurnal tide with a downwards propagating anomaly of 2–4 K, from approximately 20 Pa at 0 hr to the surface at 16 hr (orange dashed line in Figure 3a). Another temperature maximum appears across all pressure levels near 15 hr, which is a sign of the semi-diurnal tide, but it is also likely introduced by the sampling scheme of TIRVIM. As the sub-spacecraft point slowly drifts in local time, and crosses each latitude twice per orbit (Figure 1a), sampling could superimpose a semi-diurnal cycle onto the temperature anomaly, as long as the background temperature keeps increasing/decreasing at certain latitudes within this season. In the case of TIRVIM observations, sampling at  $\sim 4$  and  $\sim 16$  hr after  $L_s = 100^\circ$  (Figure 1a) can solely result in such a daily temperature anomaly even if there are no thermal tides.

Outputs of the LMD Mars GCM binned over  $L_s = 75^\circ$ – $105^\circ$  are used for comparison (Figure 3b). The model prediction shows a similar downward anomaly phase propagation, and an above-average temperature at 30 Pa in the early afternoon. The observation scheme is important in this investigation. When the model results are sampled at the same locations and times as the observations, the early morning temperature maximum becomes much larger ( $> 10$  K), and the early afternoon anomaly extends to a much larger pressure range (Figure 3c). This agrees with the scenario that observation sampling amplifies the “apparent” semi-diurnal variation. Nadir sounding vertical convolution (Figure 1d), another factor introduced by observations, smooths temperature profiles and therefore the anomalies (Figure 3d). The final result shows good agreement with observations (Figure 3a) including the 2–4 K “apparent” amplitude of the downwards propagating anomaly, and the anomaly in the early afternoon extending to all pressure levels. Nevertheless, two differences are noticeable. First, the model has a

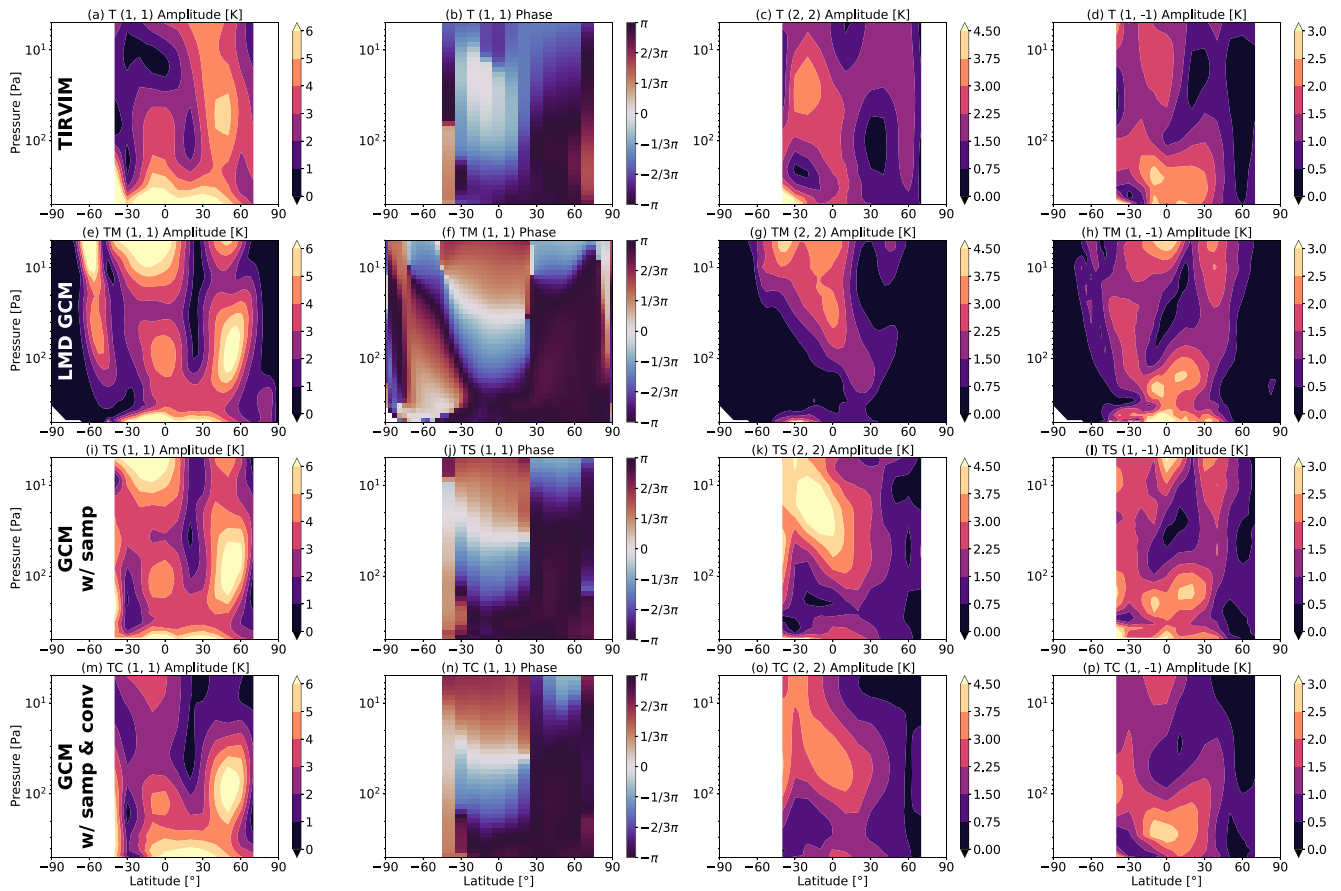


**Figure 4.** (a) Amplitude of the diurnal tide component derived from the wave mode decomposition using TIRVIM observations. (b) Same as (a), but for the phase of the diurnal tide. (c) Same as (a), but for the semi-diurnal tide. (d) Same as (a), but for the diurnal Kelvin wave. (e–h) Same as (a–d), respectively, but for the Laboratoire de Météorologie Dynamique Mars General Circulation Model outputs. (i–l) Same as (e–h), respectively, but for the model outputs sampled at the same locations and times as TIRVIM observations. (m–p) Same as (i–l), respectively, but it includes the effect of vertical convection.

phase difference of the diurnal thermal tide (blue dashed line in Figure 3d), which is  $\sim 1$  hr later than the observation. Second, the early afternoon anomaly extends more in the observation than the model, which is an indication of a larger amplitude and/or a phase difference of semi-diurnal tide than expected. This is assessed more quantitatively in Section 3.3.

### 3.3. Amplitude and Phase of Wave Mode

To investigate the contribution of wave modes, least-square fit using Equation 1 is applied to temperature observations at each latitude bin and pressure level, then amplitudes and phases of these wave modes are derived using Equations 2 and 3. An example of the decomposition in the equatorial region at 100 Pa is given in Text S2 and Figure S1 in Supporting Information S1. Three wave modes are identified important: (a) the diurnal tide, the (1, 1) mode, which propagates westwards and sun-synchronously with wavenumber one in longitude, (b) the semi-diurnal tide, the (2, 2) mode, which also propagates westwards and sun-synchronously but with a wavenumber two in longitude, and (c) the diurnal Kelvin wave, the (1, -1) mode, which propagates eastwards with wavenumber one in longitude and with a period of one Martian day. Distributions of wave mode amplitudes and phases are then computed by applying the decomposition to each latitude bin and pressure level. The results are shown in Figure 4 for the retrieved TIRVIM temperature profiles (Figures 4a–4d), the original model outputs (Figures 4e–4h), the model outputs with the same sampling as observations (Figures 4i–4l), and with the same sampling as well as the vertical convection (Figures 4m–4p). Consistency of the resulting amplitudes and phases indicates the success of the decomposition, as the implementation of decomposition is independent at each latitude and pressure level. Also, the derived background temperatures, the (0, 0) mode (the first column of Figure

S2 in Supporting Information S1), have good agreements with their corresponding zonal mean values computed using binned data (Figure 2) without any visible differences.

The amplitude distribution of diurnal tide shows a good agreement between observations (Figure 4a) and the model (Figure 4e). At  $\sim 50$  Pa, it has a large maximal value ( $\sim 5$  K) at  $\sim 50^\circ\text{N}$ , and a smaller local maximum near the equator, while possible amplitude maxima at  $\sim 5$  Pa are smoothed out by the vertical convolution (Figures 4i and 4m). The overall structure of the observed phase distribution has a fairly good agreement with model prediction, both of which show consistent downward progression (Figures 4b and 4f). Noticeable differences are in the equatorial region at pressure levels less than  $\sim 30$  Pa. This is likely due to the small derived amplitude (Figure 4a), which results in the difficulty of determining the phase.

In contrast to the diurnal tide, the latitude-pressure structure of the semi-diurnal tide shows significant disagreements between observations and the model, except for the fact that they have similar maximal amplitudes of  $\sim 3$  K (Figures 4c and 4g). The observation scheme is important in this case. The shape of the structure becomes much similar when the model is sampled at the same locations and times as observations, but it meanwhile introduces larger “apparent” amplitude (Figure 4k). Vertical convolution smooths temperature gradients and therefore the derived tide amplitudes, which results in a much better agreement between the final model prediction (Figure 4o) and the observation (Figure 4c). This is consistent with the scenario described in Section 3.2. The phase of the semi-diurnal tide shows generally good agreements (the second column in Figure S2 in Supporting Information S1). Both observation and the model show downward phase progression, which is almost linear with the logarithm of pressure from 5 to 100 Pa (Figure S3 in Supporting Information S1). Vertical wavelength of the semi-diurnal tide can therefore be derived by a linear fit to the phase progression, which is  $\sim 60$  km in the model if assuming a scale height of 10 km, but it is  $\sim 90$  km when the observation scheme is considered. The observations show a good agreement in the wavelength, but it is earlier by  $\sim \pi/4$  (3 hr in local time), which potentially explains the different early afternoon anomaly shown in Figure 3.

Despite a smaller amplitude, the  $(1, -1)$  diurnal Kelvin wave is successfully distinguished. It has an amplitude maximum of  $\sim 2.5$  K at  $\sim 200$  Pa, indicated by both observations and the model (Figures 4d and 4h), and also a possible maximum at  $\sim 5$  Pa (Figure 4h), which is likely smoothed out by the vertical convolution (Figure 4p). The phase of the Kelvin wave also agrees between observations and the model (Figures S2c and S2o in Supporting Information S1) if the observation scheme is taken into consideration. Interpretation of this mode is not influenced by the sampling scheme (Figures 4h and 4i), as it propagates eastwards, the other direction than sun-synchronous. Another mode, the  $(1, 0)$  stationary wave, is expected to be important at latitudes south of  $45^\circ\text{S}$  (Figure S2h in Supporting Information S1), but it is not seen from the observations due to limited data coverage (Figure 1b).

#### 4. Discussion and Conclusion

In this work, temperature in the Martian atmosphere is analyzed across multiple local times using profiles retrieved from nadir-viewing spectra obtained by TIRVIM during a dust-free season,  $L_s = 75^\circ\text{--}105^\circ$  of MY 35. TIRVIM observations show dominant diurnal tide and important semi-diurnal tide and Kelvin wave, with influence from observation strategy. They agree with predictions made by the LMD Mars GCM, but with phases of diurnal and semi-diurnal tides earlier than expected.

Diurnal temperature variations in the Martian atmosphere are analyzed using observations with full local time coverage for the first time. No assumptions about the latitudinal distributions of atmospheric wave modes, or the Hough modes (Lindzen & Chapman, 1969), whose characteristics depend on more assumptions about the physical properties of the Martian atmosphere, are required in the wave mode analysis. This was inevitable in previous works using observations from TES or MCS (e.g., Wilson, 2000; Guzewich et al., 2012). Due to the full coverage of local time, phases of the wave modes are well constrained. The dominant diurnal tide has a phase varying from 0 to  $-(1/2)\pi$  within a wide pressure range ( $\sim 50\text{--}200$  Pa, Figure 4b), which corresponds to its wave crest being in late morning. This suggests that the temperature differences computed at the sampling local times of TES and MCS (Banfield et al., 2000; Lee et al., 2009) within this pressure range are likely smaller than the actual tide amplitude. The amplitude of the semi-diurnal tide has a maximum near the equator and is observed to reach 2–3 K in the lower atmosphere  $>5$  Pa, which agrees well with previous works during the same season (e.g., Banfield et al., 2000; Kleinböhl et al., 2013). However, the phase is earlier by  $\sim 3$  hr than expected. Reasons

leading to such a phase difference, as well as that for the diurnal tide, are currently unknown. Preliminary investigation using the GCM suggests that phases of modeled tides are not sensitive to parameters included in the current model, which indicates that the phase discrepancy is significant and presents a challenge to numerical simulations. The local time coverage also allows an investigation of the ter-diurnal tide, the (3, 3) mode, which is tested by expanding the truncation of  $\sigma$  to  $\pm 3$  in Equation 1. This results in 49 linearly independent unknowns in the wave mode decomposition. However, the results suggest that this mode is not important, at least during this season, with an amplitude of  $<0.5$  K in most of the cases (Figure S4 in Supporting Information S1).

Two sources of degeneracy, vertical convolution and sampling scheme, largely influence the interpretation of thermal tides using TIRVIM observations. The vertical convolution originates from the nadir viewing geometry thermal sounding. It smooths the temperature vertical oscillations and therefore reduces the apparent daily anomaly. A comparison of these temperature profiles with those obtained from limb sounding by MCS (Kleinböhl et al., 2009) is presented in Guerlet et al. (2022), where two sets of profiles show good agreement when vertical convolution is included. This is consistent with the model-observation agreement shown in this work. The sampling strategy of local time is also important due to the slow drift of the observation local time (Figure 1a), which results in the modulation of seasonal temperature variations into daily temperature anomalies. As the seasonal changes can have large values, for example, a  $\sim 2$  K increase in the equatorial region at 30 Pa suggested by the GCM, a small difference in  $L_S$  ( $\sim 20^\circ$  in the case of this work) could result in noticeable amplification of decomposed tides. This effect has larger influences on the interpretation of migrating than non-migrating tides, so the model-observation agreement is better for the diurnal Kelvin wave than the diurnal and semi-diurnal tides (Figure 4). Obtaining a full local time coverage within a short seasonal range is helpful to address this issue. Observations from the Emirates Mars Infrared Spectrometer (EMIRS, Edwards et al., 2021) onboard the Hope spacecraft are expected to provide promising results, with the capability of sampling all local times at a given region over 10 sols.

## Data Availability Statement

The TIRVIM retrieval results used in this paper are available on the Institut Pierre Simon Laplace (IPSL) data server with doi: [10.14768/ab765eba-0c1d-47b6-97d6-6390c63f0197](https://doi.org/10.14768/ab765eba-0c1d-47b6-97d6-6390c63f0197). The LMD Mars GCM output during  $L_S = 60^\circ$ – $120^\circ$  of MY 35 is also available on the IPSL data server with doi: [10.14768/9853d6ae-7d11-450f-9363-ac8cf7bd143a](https://doi.org/10.14768/9853d6ae-7d11-450f-9363-ac8cf7bd143a). Permission is granted to use these datasets in research and publications with appropriate acknowledgements that are presented on the data set websites.

## Acknowledgments

This work was supported by CNES. It is based on observations with ACS/TIRVIM embarked on TGO. The science operations of ACS are funded by Roscosmos and ESA. The TIRVIM team at IKI acknowledges the subsidy of the Ministry of Science and High Education of Russia.

## References

- Banfield, D., Conrath, B., Pearl, J. C., Smith, M. D., & Christensen, P. (2000). Thermal tides and stationary waves on Mars as revealed by Mars Global Surveyor thermal emission spectrometer. *Journal of Geophysical Research*, *105*(E4), 9521–9537. <https://doi.org/10.1029/1999JE001161>
- Capderou, M., & Forget, F. (2004). Optimal orbits for Mars atmosphere remote sensing. *Planetary and Space Science*, *52*(9), 789–798. <https://doi.org/10.1016/j.pss.2004.03.006>
- Edwards, C. S., Christensen, P. R., Mehall, G. L., Anwar, S., Tunajji, E. A., Badri, K., et al. (2021). The Emirates Mars mission (EMM) Emirates Mars InfraRed spectrometer (EMIRS) instrument. *Space Science Reviews*, *217*(7), 77. <https://doi.org/10.1007/s11214-021-00848-1>
- Fan, S. (2022). LMD Mars GCM for MY 35 LS 60–120 [Data set]. IPSL. <https://doi.org/10.14768/9853d6ae-7d11-450f-9363-ac8cf7bd143a>
- Forbes, J. M., Zhang, X., Forget, F., Millour, E., & Kleinböhl, A. (2020). Solar tides in the middle and upper atmosphere of Mars. *Journal of Geophysical Research: Space Physics*, *125*(9), e28140. <https://doi.org/10.1029/2020JA028140>
- Forget, F., Hourdin, F., Fournier, R., Hourdin, C., Talagrand, O., Collins, M., et al. (1999). Improved general circulation models of the Martian atmosphere from the surface to above 80 km. *Journal of Geophysical Research*, *104*(E10), 24155–24176. <https://doi.org/10.1029/1999JE001025>
- Gierasch, P., & Goody, R. (1968). A study of the thermal and dynamical structure of the Martian lower atmosphere. *Planetary and Space Science*, *16*(5), 615–646. [https://doi.org/10.1016/0032-0633\(68\)90102-5](https://doi.org/10.1016/0032-0633(68)90102-5)
- Giuranna, M., Wolkenberg, P., Grassi, D., Aronica, A., Aoki, S., Scaccabarozzi, D., et al. (2021). The current weather and climate of Mars: 12 years of atmospheric monitoring by the planetary Fourier spectrometer on Mars express. *Icarus*, *353*, 113406. <https://doi.org/10.1016/j.icarus.2019.113406>
- Guerlet, S. (2021). ACS/TIRVIM temperature and aerosol retrievals [Data set]. IPSL. <https://doi.org/10.14768/ab765eba-0c1d-47b6-97d6-6390c63f0197>
- Guerlet, S., Ignatiev, N., Forget, F., Fouchet, T., Vlasov, P., Bergeron, G., et al. (2022). Thermal structure and aerosols in Mars' atmosphere from TIRVIM/ACS onboard the ExoMars Trace Gas Orbiter: Validation of the retrieval algorithm and application to early observations. *Journal of Geophysical Research: Planets*, *127*, e2021JE007062. <https://doi.org/10.1029/2021JE007062>
- Guzewich, S. D., Talaat, E. R., & Waugh, D. W. (2012). Observations of planetary waves and nonmigrating tides by the Mars Climate Sounder. *Journal of Geophysical Research*, *117*, E03010. <https://doi.org/10.1029/2011JE003924>
- Hess, S. L., Henry, R. M., Leovy, C. B., Ryan, J. A., & Tillman, J. E. (1977). Meteorological results from the surface of Mars: Viking 1 and 2. *Journal of Geophysical Research*, *82*(B28), 4559–4574. <https://doi.org/10.1029/J082i028p04559>

- Kleinböhl, A., John Wilson, R., Kass, D., Schofield, J. T., & McCleese, D. J. (2013). The semidiurnal tide in the middle atmosphere of Mars. *Geophysical Research Letters*, *40*(10), 1952–1959. <https://doi.org/10.1002/grl.50497>
- Kleinböhl, A., Schofield, J. T., Kass, D. M., Abdou, W. A., Backus, C. R., Sen, B., et al. (2009). Mars Climate Sounder limb profile retrieval of atmospheric temperature, pressure, and dust and water ice opacity. *Journal of Geophysical Research*, *114*, E10006. <https://doi.org/10.1029/2009JE003358>
- Korablev, O., Montmessin, F., Trokhimovskiy, A., Fedorova, A. A., Shakun, A. V., Grigoriev, A. V., et al. (2018). The atmospheric Chemistry suite (ACS) of three spectrometers for the ExoMars 2016 Trace Gas orbiter. *Space Science Reviews*, *214*(1), 7. <https://doi.org/10.1007/s11214-017-0437-6>
- Lee, C., Lawson, W. G., Richardson, M. I., Heavens, N. G., Kleinböhl, A., Banfield, D., et al. (2009). Thermal tides in the Martian middle atmosphere as seen by the Mars Climate Sounder. *Journal of Geophysical Research*, *114*(E3), E03005. <https://doi.org/10.1029/2008JE003285>
- Lindzen, R. S., & Chapman, S. (1969). Atmospheric tides. *Space Science Reviews*, *10*(1), 3–188. <https://doi.org/10.1007/BF00171584>
- Navarro, T., Forget, F., Millour, E., Greybush, S. J., Kalnay, E., & Miyoshi, T. (2017). The challenge of atmospheric data assimilation on Mars. *Earth and Space Science*, *4*, 690–722. <https://doi.org/10.1002/2017EA000274>
- Svedhem, H., Korablev, O., Mitrofanov, I., Rodionov, D., Thomas, N., Carine Vandaele, A., et al. (2020). *The ExoMars Trace Gas orbiter - first martian year in orbit*. European Planetary Science Congress, 802.
- Wilson, R. J. (2000). Evidence for diurnal period Kelvin waves in the Martian atmosphere from Mars Global Surveyor TES data. *Geophysical Research Letters*, *27*(23), 3889–3892. <https://doi.org/10.1029/2000GL012028>
- Wu, Z., Li, T., & Dou, X. (2015). Seasonal variation of Martian middle atmosphere tides observed by the Mars Climate Sounder. *Journal of Geophysical Research: Planets*, *120*(12), 2206–2223. <https://doi.org/10.1002/2015JE004922>
- Wu, Z., Li, T., & Dou, X. (2017). What causes seasonal variation of migrating diurnal tide observed by the Mars Climate Sounder? *Journal of Geophysical Research: Planets*, *122*(6), 1227–1242. <https://doi.org/10.1002/2017JE005277>
- Zurek, R. W. (1976). Diurnal tide in the Martian atmosphere. *Journal of the Atmospheric Sciences*, *33*, 321–337. [https://doi.org/10.1175/1520-0469\(1976\)033<0321:ditma>2.0.co;2](https://doi.org/10.1175/1520-0469(1976)033<0321:ditma>2.0.co;2)

## Reference From the Supporting Information

- Montabone, L., Spiga, A., Kass, D. M., Kleinboehl, A., Forget, F., & Millour, E. (2020). Martian year 34 column dust climatology from Mars climate sounder observations: Reconstructed maps and model simulations. *Journal of Geophysical Research: Planets*, *125*, e2019JE006111. <https://doi.org/10.1029/2019JE006111>